

Supporting Information for:

Towards a better understanding of the origins, the chemical composition and the aging of the Oxygenated Organic Aerosol: case study of a Mediterranean Industrialized Environment, Marseille

Imad El Haddad ^{a,1,*}, Barbara D'Anna ^b, Brice Temime-Roussel ^a, Melanie Nicolas ^b,
Antoinette Boreave ^b, Olivier Favez ^{b,2}, Didier Voisin ^c, Jean Sciare ^d, Christian George ^b,
Jean-Luc Jaffrezo ^c, Henri Wortham ^a, and Nicolas Marchand ^{a,*}

^a Aix-Marseille Univ, Laboratoire Chimie Environnement, 13331, Marseille cedex 03, France

^b Université Lyon 1, Lyon, F-69626, France; CNRS, UMR5256, IRCELYON, Institut de Recherches sur la Catalyse et l'Environnement de Lyon, Villeurbanne, F-69626, France

^c Universités Joseph Fourier-Grenoble 1-CNRS, UMR 5183, Laboratoire de Glaciologie et Géophysique de l'Environnement, Saint Martin d'Hères, 38402, France.

^d Laboratoire des Sciences du Climat et de l'Environnement, CEA-CNRS-UVSQ-IPSL, Gif sur Yvette, 91191, France.

¹Now at Laboratory of Atmospheric Chemistry, Paul Scherrer Institut, 5232 Villigen PSI, Switzerland.

²Now at INERIS, DRC/CARA/CIME, Parc Technologique Alata, BP2, Verneuil-en-Halatte, 60550, France.

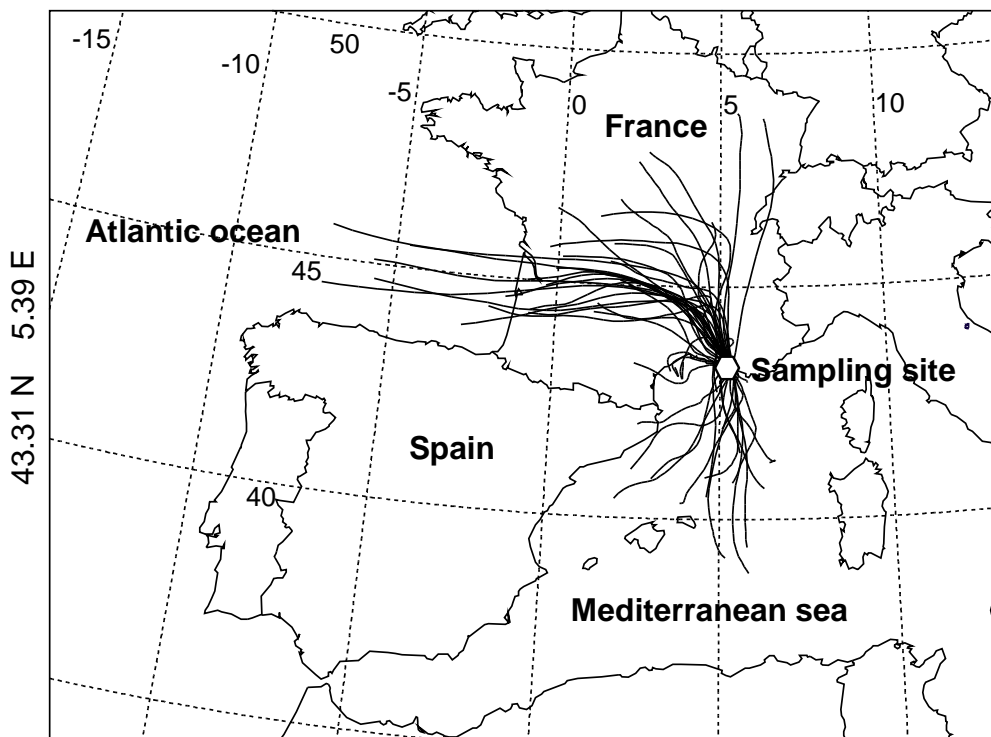
* Corresponding authors:

I. El Haddad – email: imad.el-haddad@psi.ch, phone: +41 5 63 10 27 85, fax: +41 5 63 10 45 25

N. Marchand – email: Nicolas.Marchand@univ-amu.fr, phone: +33 4 13 55 10 51, fax: +33 4 13 55 10 60

24 **S.1 Synoptic air masses**

25 Fig.S1 illustrates the air masses impacting the sampling site during the measurement
26 period and shows that these air masses are mostly associated with long range transport
27 from the Atlantic and the Mediterranean.

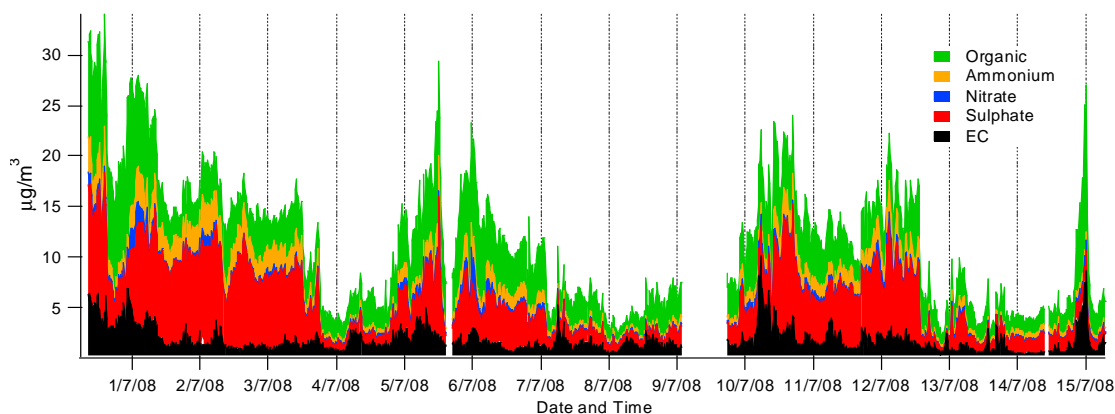


28 **Fig.S1:** 24h HYSPLIT air masses backward trajectories at 100m above sea level (Rolph, 2010)
29 illustrating the overall air masses circulation occurring during the entire measurement campaign.
30 Backward trajectories are confirmed by both MM5 modeling and local wind measurements.
31

32 **S.2 Aerosol online chemical composition**

33 The chemical composition of fine PM was measured in 2 min averages using a compact
34 time-of-flight (c-TOF, ToFwerk) Aerodyne Aerosol Mass Spectrometer (AMS,
35 Aerodyne). This instrument allows real-time measurements of PM₁ non-refractory
36 components (OA, NH₄, NO₃ and SO₄) combining thermal vaporization and electron
37 ionization (Drewnick et al., 2005). Aerosol size distribution (mobility diameters from 11
38 to 1083 nm), was investigated using a Scanning Mobility Particle Sizer (SMPS, L-DMA
39 and CPC5403, GRIMM). Semi-continuous hourly concentrations of elemental carbon
40 (EC) and organic carbon (OC) PM_{2.5} were obtained in the field from an OC/EC Sunset
41 field instrument (Sunset Laboratory, Forest Grove, OR, USA; Bae et al., 2004) running at
42 81 min⁻¹. AMS results are all corrected for the collection efficiency by using a common

43 factor of 0.65 ± 0.14 estimated based on the comparison of total AMS measured mass and
44 SMPS + EC measured mass. Fig.S2 displays EC, OA, NH_4 , NO_3 and SO_4 time series
45 recorded over the period of study.



46 **Fig.S2:** Time series of the main PM_{10} components (EC, OA, NH_4 , NO_3 and SO_4) during the
47 period of study. AMS data are corrected for the collection efficiency using a common factor of
48 0.65 ± 0.14 . Due to technical issues, AMS measurements are not available between the 9th and 10th
49 of July.
50

51 S.3 Offline chemical analyses

52 $\text{PM}_{2.5}$ collected onto 150 mm-diameter filters was comprehensively characterized.
53 Technical description of the analysis techniques can be found in El Haddad et al., 2011a
54 and b. A brief outline of these measurements is included here.

55 EC/OC, ions, WSOC, HULIS_{WS} and elements: The carbonaceous content was analyzed
56 for EC and OC using a Thermo-Optical Transmission method on a Sunset Lab analyzer
57 (Birch and Cary, 1996), following both NIOSH (Schmid et al., 2001) and EUSAAR-2
58 (Cavalli et al., 2010) protocols. It is well established that different protocols result in very
59 different values for EC (Schmid et al., 2001). We based our analysis (i.e., Chemical Mass
60 Balance analysis and multiple regression analysis, see below sections S.4 and S.9) on
61 concentrations determined following NIOSH protocol, as source profiles were
62 determined based on this protocol. Biases arising from discrepancies between the two
63 protocols are all discussed in S.9.2 of the supporting material.

64 Sample fractions of 11.34 cm^2 taken from the sample filter were extracted into 15 mL
65 ultrapure Milli-Q water by 30 min short vortex agitation for the analyses of major ions
66 (NH_4^+ , SO_4^{2-} , NO_3^-), water-soluble organic carbon (WSOC) and water-soluble humic like
67 substances (HULIS). HULIS analysis was performed following the method described in

68 Baduel et al. (2009, 2010). This method involves extraction of HULIS by adsorption onto
69 DEAE resin (GE Healthcare®, HiTrap™ DEAE FF, 0.7 cm ID×2.5 cm length) and its
70 subsequent quantification with an OI Analytical 700 total organic carbon analyzer.

71 Finally, fifty elements were measured using ICP-MS (Agilent 7500ce) following the
72 complete dissolution of filter aliquots in a mixture of high-purity concentrated HF and
73 HNO₃. Element concentrations were then calculated using the rock reference material BR
74 (Chauvel et al., 2010).

75 Radiocarbon measurements: Radiocarbon (¹⁴C) measurements were conducted on high
76 volume quartz filter fractions (~40 cm²) using ARTEMIS Accelerator Mass
77 Spectrometry. Each sample was first packed into a pre-fired quartz tube containing CuO
78 and Ag powder to be combusted at 850°C in a muffle furnace for 4 hours. Carbon dioxide
79 was collected and purified before its conversion into graphite by hydrogen reduction at
80 600°C using an Fe catalyst. The modern fraction (f_m) was determined as the ratio of
81 ¹⁴C/¹²C in aerosol sample to ¹⁴C/¹²C in the NBS Oxalic Acid standard (NIST-SRM-
82 4990B).

83 In order to account for the thermonuclear weapon tests of the late 1950s and early 1960s
84 (Levin et al., 1985), the modern fraction (f_m) is divided by a ratio of 1.1 to get a corrected
85 non-fossil fraction (f_{nf}) (Levin and Hesshaimer, 2000). This value is subsequently
86 subtracted from one to obtain the fossil fraction (f_f).

87 Organic speciation: A chemical derivatisation/gas chromatography-mass spectrometry
88 (GC-MS) approach was used to quantify primary and secondary organic markers,
89 including α-pinene oxidation products, a major focus of this study. The approach is fully
90 described in El Haddad et al., 2011b and will be only outlined in the following.

91 Prior to extraction, filters were spiked with known amounts of two isotope-labelled
92 standards: tetracosane-d50 and cholesterol-d6. Organic species were extracted from
93 filters with a dichloromethane/acetone mix (1/1 v:v) using an accelerated pressurized
94 solvent extraction device (ASE, Dionex 300). Extracts were then reduced to a volume of
95 500µL using a Turbo Vap II concentrator. The remainder was split into two fractions.
96 The first fraction was directly injected, whilst the second fraction was subjected to
97 derivatization for 2 h at 70 °C, using N,O-Bis(trimethylsilyl)-trifluoroacetamide containing
98 10% trimethyl-chlorosilane ,before GC-MS analysis. The two fractions were analyzed

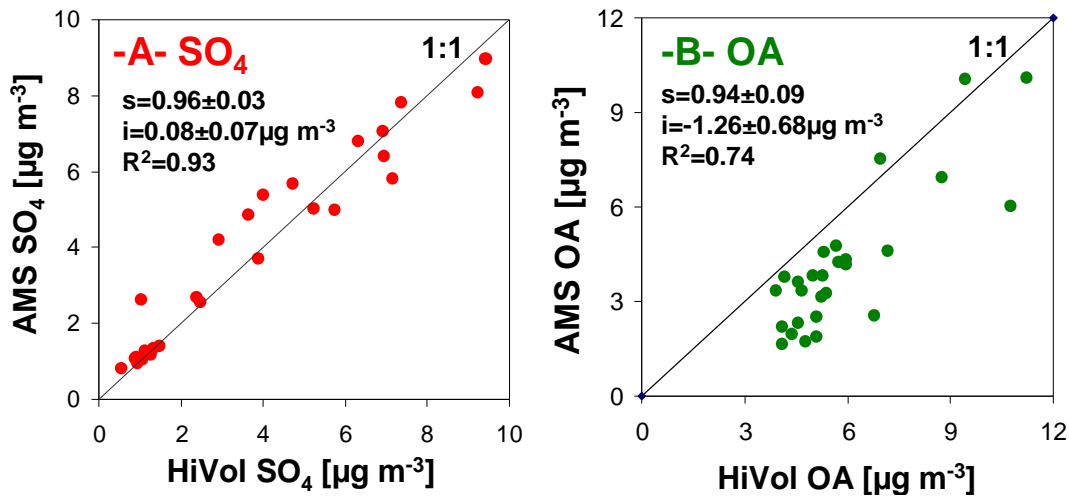
99 following the same GC-MS conditions: Aliquots of 2 μ L were analyzed using a Thermo
100 Trace GC chromatograph interfaced to a Polaris Q ion trap mass spectrometer fitted with
101 an external electron ionization source. The chromatographic separation was accomplished
102 on a TR-5MS capillary column (Thermo Electron, 30 m \times 0.25 mm i.d. \times 0.25 μ m film
103 thickness). Field blank filters were also treated with the same procedure and none of the
104 target compounds were detected in these field blanks.

105 Primary organic markers, including n-alkanes, hopanes, polycyclic aromatic hydrocarbon
106 (PAH) and levoglucosan, were quantified and used as inputs in the CMB analysis to
107 apportion primary aerosol and VOC sources. A complete list of these primary organic
108 markers is included in El Haddad al. (2011a). α -pinene oxidation products quantified by
109 this method were used to estimate α -pinene SOA contributions. As described in El
110 Haddad al. (2011b), we identified and quantified 9 α -pinene SOA markers, whose
111 structures are presented in Fig.2. These included pinic (PA) and pinonic (PNA) acid,
112 which were identified and quantified using authentic standards. Seven other
113 multifunctional compounds (A1-A7), for which native standards are not available, were
114 tentatively identified by examining their retention times and MS characteristics (for more
115 details refer to El Haddad et al., 2011b). They included 3-hydroxyglutaric acid (A1), 3-
116 (2-hydroxyethyl)-2,2-dimethylcyclobutane carboxylic acid (A2), 3-hydroxy-4,4-
117 dimethylglutaric acid (A3), 3-acetylglutaric acid (A4), 3-acetyladipic acid (A5), and 3-
118 isopropylglutaric acid (A6) and 3-methyl-1,2,3-butanetricarboxylic (A7). These
119 compounds were quantified using the response factor of malic acid as a surrogate for all
120 of the compounds. Relative standard deviation of the concentrations of these species
121 based on duplicate analysis was between 5 and 15%.

122 **S.4 Comparison between offline and online measurements**

123 The aim of this section is to evaluate biases and artefacts associated with the offline and
124 online measurements of OA (e.g., AMS particle collection efficiency, adsorption artefacts
125 onto filters). Fig.S3 conveys the comparison between AMS (PM_{10}) and filter based
126 ($PM_{2.5}$) measurements for the two major aerosol components: SO_4 and OA. SO_4 is
127 expected to primarily occur in the PM_{10} fraction and to be mostly associated with
128 ammonium sulfate and bisulfate (with very little influence from sea salt), and thus to be
129 quantitatively analysed by the AMS. A very good agreement was observed between the

130 AMS-SO₄ and the HiVol-SO₄ ($s \sim 1$, $i \sim 0$ and $R^2 > 0.9$; Fig.S3), substantiating our AMS
 131 measurements and the particle collection efficiency factor, HiVol-OA was derived from
 132 OC concentrations measured from filter samples, corrected for differences in diameter
 133 cut-offs between the AMS and the HiVol sampler; **it constitutes our best estimate of**
 134 **offline PM₁OA.**



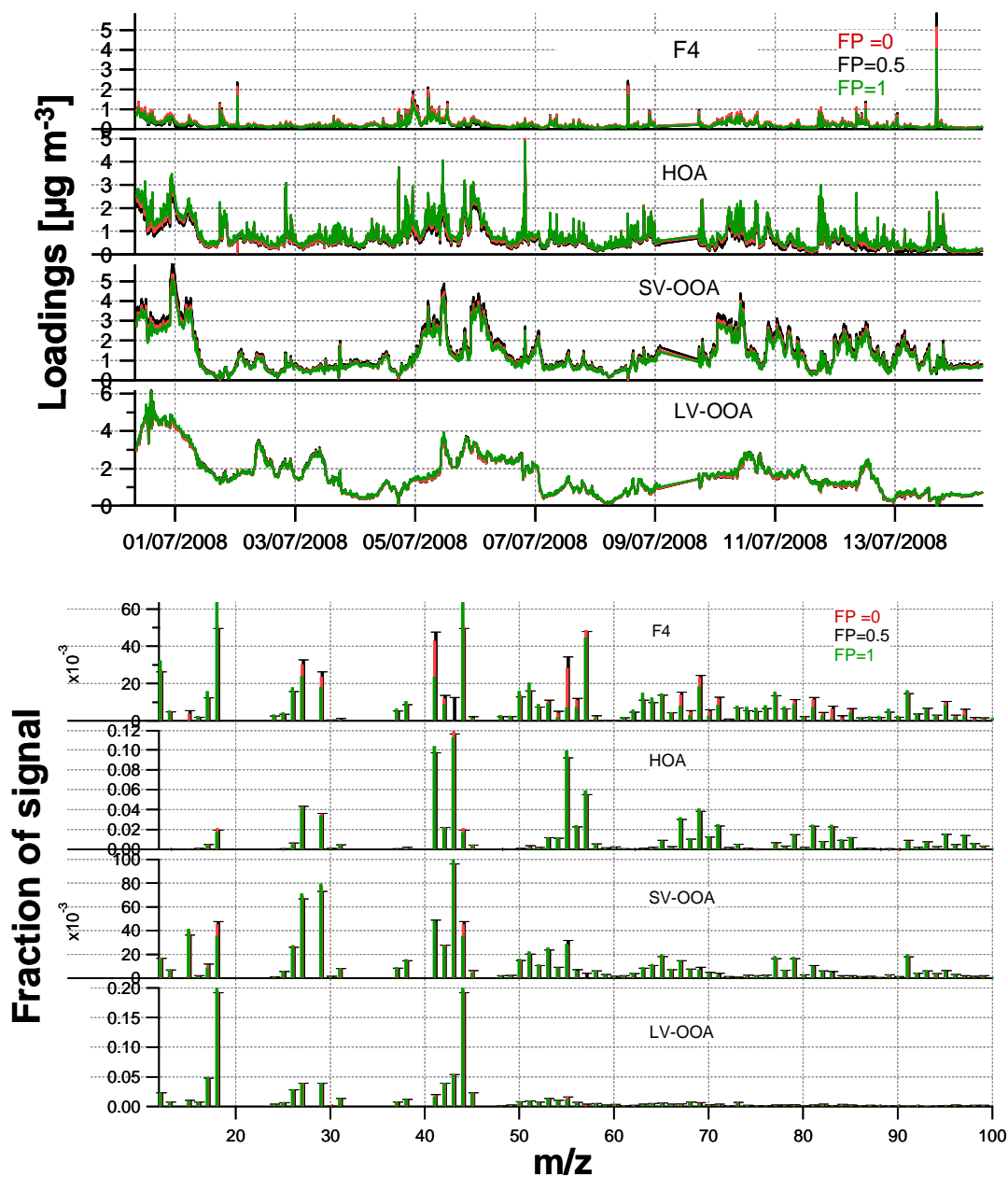
135
 136 **Fig.S3:** Comparison between AMS and offline measurements for SO₄ (A) and OA (B). HiVol-
 137 OA was corrected for differences in the diameter cut-offs between the AMS and the HiVol
 138 sampler (see text); it refers to the PM₁ fraction. Also shown are the 1:1 line and the slopes (s),
 139 intercepts (i) and coefficients of determination (R^2) obtained by linear fits of the data.

140 The calculation of PM₁OA proceeded as follows: Based on size resolved EC/OC
 141 measurements performed on the LPI samples, the fraction of PM₁OC in PM_{2.5}OC was
 142 retrieved: $PM_1OC/PM_{2.5}OC = 0.82 \pm 0.06$. PM₁OC was then scaled by an average
 143 OM/OC ratio of 1.67 ± 0.05 , obtained by comparing the AMS-OA to the LPI PM₁OC. The
 144 comparison between PM₁OA and AMS-OA shows that both fractions exhibit similar
 145 variability ($R^2 > 0.7$), with a slope close to 1. However, a negative intercept of $-1.3 \pm 0.7 \mu\text{g}$
 146 m^{-3} was observed, implying that filter based measurements (PM₁OA) were systematically
 147 associated with a positive bias of $1.3 \mu\text{g m}^{-3}$ engendered by adsorption artefacts onto
 148 filter samples. As a result, filter based measurements tended to overestimate the absolute
 149 concentrations of OA by up to 28%[†]. However, such artefacts would have only a minor

[†] The following estimation of adsorption artefacts onto HiVol filter samples (positive artefacts of 28%) is obtained by assuming first no volatilisation artefacts occurred during sampling with the LPI and second a quantitative transmission and evaporation of PM₁ organic particles in the AMS. Negative artefacts are common for sampling under low pressure and losses and slow vaporisation of large particles can be an issue in the AMS. Therefore, our estimation of positive artefacts onto the HiVol samples should be regarded as highest estimate.,

150 influence on our apportionments, provided that they evenly impacted the different
151 components of OA.

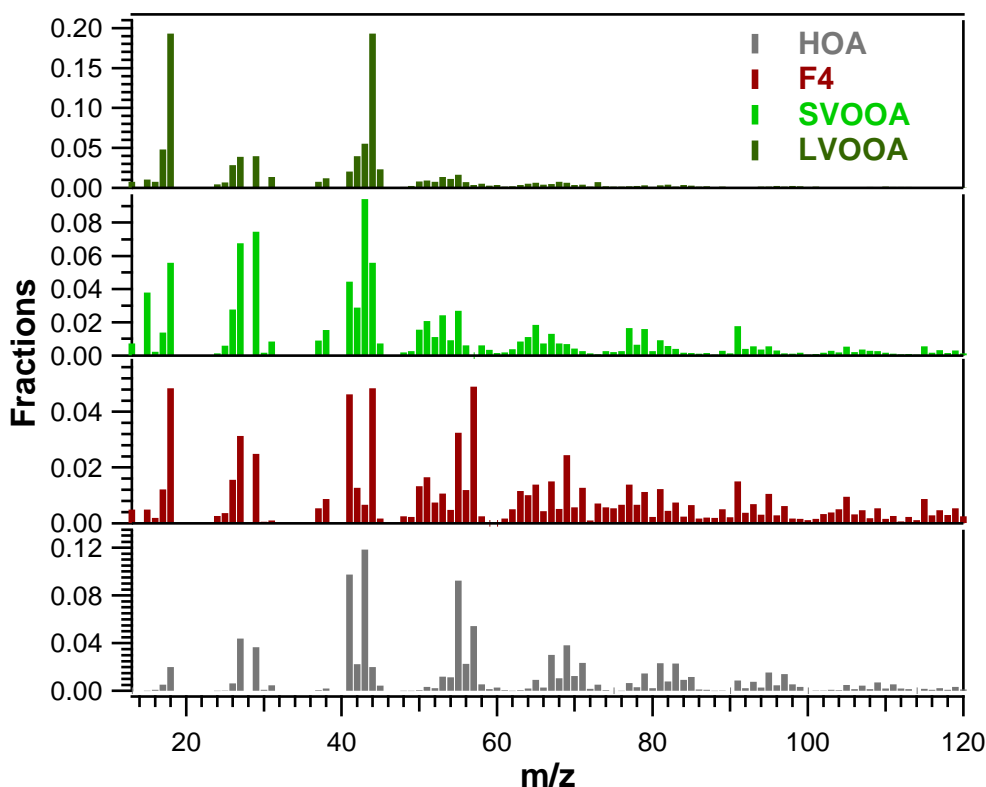
152 S.5 AMS/PMF2 analysis



153
154 **Fig.S4:** Influence of varying FPEAK parameter on factors' mass spectra and time series for the
155 4-factor solution and at FPEAKs between 0 and 1.

156 To assess the robustness of the 4 factor solution, rotational ambiguity has been
157 investigated by varying FPEAK from -2 to 2 with 0.1 steps. Two main groups of
158 solutions were identified, the first one corresponding to FPEAK values below 0, for

159 which unrealistic zero time series values are observed for LVOOA, and the other one
 160 corresponding to “FPEAK” above 0. Robust solutions were found for solutions at
 161 FPEAK between 0 to 1, with very little variability in the factors’ time series and mass
 162 spectra (Fig.S4). The influence of the initial conditions seed (corresponding to
 163 pseudorandom starting-points of the PMF2 algorithm) ranging from 0 to 59 (with steps of
 164 1) was also verified. No influence of different seed was observed, which provides
 165 evidence of the robustness of the chosen solution.



166
 167 **Fig.S5:** Factor spectral profiles derived from the 4 factor solution PMF2 analysis for FPEAK 0
 168 and seed=0.

169 **S.6 Chemical Mass Balance analysis**

170 Available data used here also included source contributions to OC, apportioned using a
 171 Chemical Mass Balance analysis (CMB) in conjunction with organic marker
 172 concentrations, as fully described in El Haddad et al. (2011a). CMB model is based on
 173 the mass conservation of individual organic markers. In the mass conservation equations,
 174 known concentrations (C_{ik}) of specific markers of primary sources at receptor site k are
 175 written as the product of known source profiles a_{ij} and unknown primary source
 176 contributions s_{jk} (Watson et al., 1998) as expressed in equation 1:

$$C_{ik} = \sum_{j=1}^m a_{ij} s_{jk} \quad (1)$$

177 where m denotes the total number of emission sources and a_{ij} represents the fractional
178 abundances of chemical species in the source emissions, expressed as marker-to-OC
179 ratios. The set of linear equations generated by equation 1 is solved with an effective
180 variance weighted least squares method using the Environmental Protection agency EPA-
181 CMB8.2 software.

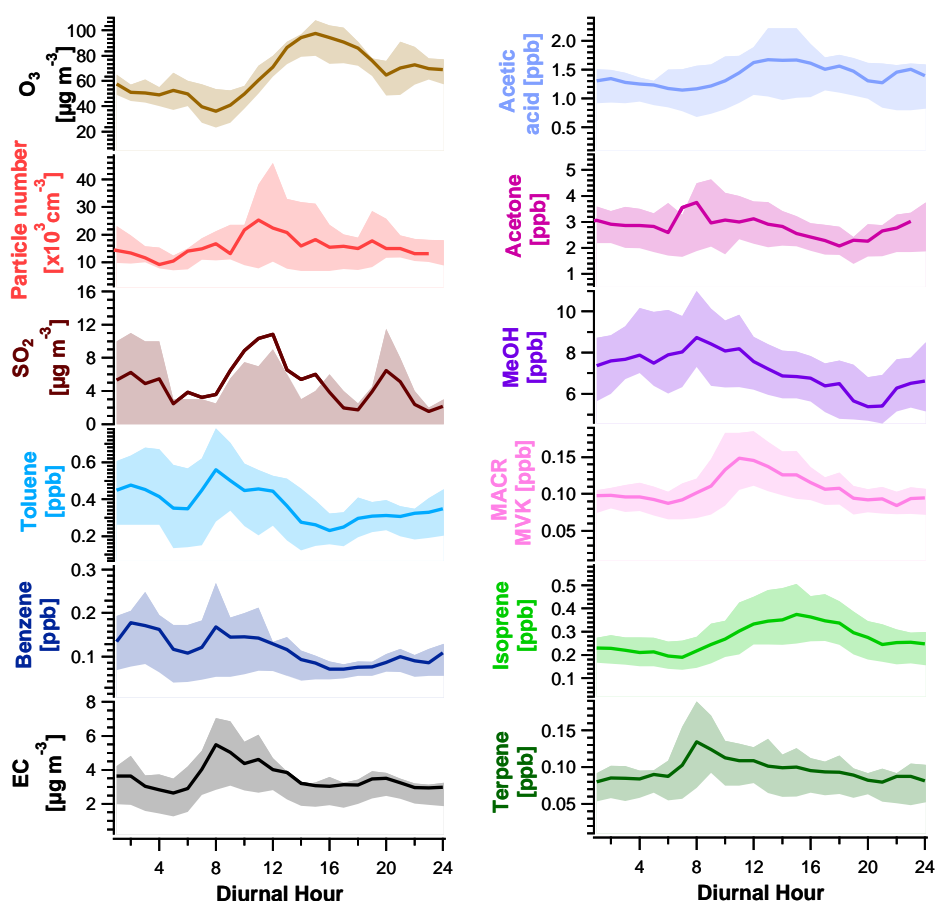
182 Primary markers and source profiles selection is detailed in El Haddad et al., 2011a.
183 Primary markers include: levoglucosan as a specific marker for biomass burning
184 (BBOC), EC and three hopanes (i.e., 17(H),21(H)-norhopane, 17(H),21(H)-hopane and
185 22S,17(H), 21 (H)-homohopane) as key markers for vehicular emissions. In addition, a
186 series of C27-C32 n-alkanes was selected since this range demonstrates high odd-carbon
187 preference, specific to primary biogenic sources. In order to apportion industrial
188 emissions, four PAH (benzo[b,k]fluoranthene, benzo[e]pyrene, indeno[1,2,3-cd]pyrene,
189 and benzo[ghi] perylene), V, Ni and Pb were included as fitting species. Source profiles
190 comprise vehicular emissions derived from a tunnel study held in Marseille (El Haddad et
191 al., 2009), biomass burning emissions (Fine et al., 2002), vegetative detritus (Rogge et al.,
192 1993a) and natural gas combustion (Rogge et al., 1993b). Three industrial-emission-
193 related profiles were chosen, including metallurgical coke production (Weitkamp et al.,
194 2005), HFO combustion/shipping (Agrawal et al., 2008), and steel manufacturing (Tsai et
195 al., 2007).

196 In this study, emissions from the three industrial processes were lumped together under
197 the term “industrial OA”. Biomass burning, vegetative detritus and natural gas
198 combustion contributed very little OC during the period of measurements (El Haddad et
199 al., 2011a) and were not considered in the comparison between CMB and AMS/PMF
200 results. CMB technique is unable to directly apportion secondary sources; however, the
201 fraction of OC not attributed to primary sources is considered to be an upper limit
202 estimate of secondary OC (SOC).

203 In order to compare CMB and AMS/PMF results, primary OA associated with vehicular
204 and industrial emissions were calculated by applying an OM-to-OC ratio of 1.2 (based on
205 Aiken et al., 2008). SOA was considered as the difference between the total OA,

206 determined by scaling the total OC by an OM-to-OC ratio of 1.67[‡], and the primary OA.
 207 An OM-to-OC ratio of 1.82 can be inferred for SOA (i.e. SOA-to-SOC), consistent with
 208 an overwhelmingly secondary origin of this fraction (Aiken et al., 2008).

209 **S.7 Tracers' diurnal profiles**



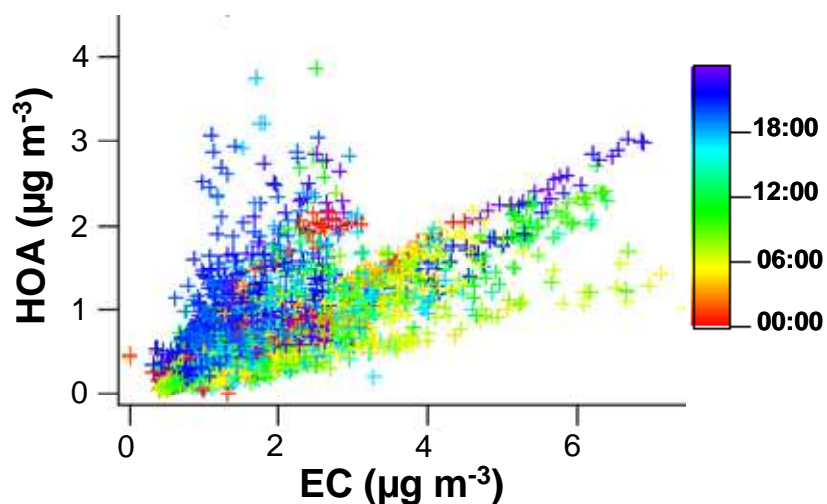
210
 211 **Fig.S6:** Tracers' diurnal profiles. Solid lines denote average profiles and shaded areas represent
 212 [P25-P75] range.

213 **S.8 HOA vs. EC**

214 Fig.S7 presents a scatter plot of HOA vs. EC, from which it is possible to ascertain more
 215 thoroughly the sources of this fraction. As HOA and EC mainly arise from the same
 216 source (i.e., vehicular emissions (El Haddad et al., 2011a)), it was expected that the data
 217 point cluster around one line with a slope corresponding to the HOA/EC ratio at the point
 218 of emission. However, more scatter was observed with three different clear patterns:

[‡] OM-to-OC ratio of 1.67 is calculated by comparing AMS OA with LPI OC measurements, see section S.3 and S.4.

219 Most of the data scattered around one line characterised by a ratio of HOA/EC of ~ 0.4 ,
220 representative of average vehicular emissions at typical ambient concentrations (see for
221 e.g. Chirico et al., 2011 and references therein). This is a clear indication that HOA was
222 mostly related to traffic. A second part of the data scattered around another line
223 characterised by a lower ratio of HOA/EC (< 0.25), concomitant with the dilution of the
224 emissions as the boundary layer developed in the afternoon and with the enhancement of
225 the photochemical activity, which would increase the oxidation of HOA. The depletion of
226 traffic emission markers with respect to EC due to photochemistry was previously
227 demonstrated to occur during this field mission (El Haddad et al., 2011a). The third part
228 of the data presents more scattering, with higher HOA/EC ratios (around 0.75), occurring
229 mostly during meal hours, especially during the evening. This suggests that the HOA
230 factor was contaminated by cooking emissions that had a similar spectral profile as HOA.
231 Based on the comparison between EC and HOA, this contamination can be estimated as
232 20%, in agreement with the very low concentrations of cholesterol ($0.13\text{--}3.32\text{ ng m}^{-3}$, El
233 Haddad et al., 2011a).



234
235

Fig.S7: HOA vs. EC. Color scale: hour of the day

236 S.9 Apportionment of fossil and non-fossil OOA and related uncertainties

237 S.9.1 Multiple regression model

238 AMS/PMF apportionments and ^{14}C measurements were combined using a multiple
239 regression model to estimate the fossil and the non-fossil contributions to both SVOOA
240 and LVOOA. It is worthwhile to note that such a combination is not straightforward,
241 involving a certain number of assumptions that result in considerable uncertainties.

242 Firstly, ^{14}C measurements were conducted on $\text{PM}_{2.5}\text{OC}$ onto filter samples that are
 243 subjected to well-known but non systematic adsorption artefacts of gas phase organic
 244 compounds. In contrast, AMS provides real-time measurements of PM_1OA with little
 245 interference from gas phase organics. However, particle collection efficiency (CE) of the
 246 AMS, estimated in this dataset to be 0.65 ± 0.14 , can be highly variable and is dependent
 247 on the aerosol chemical nature and mixing state (Middlebrook et al., 2012).

248 Secondly, ^{14}C measurements conducted in this study relate to the total carbon (TC) mass
 249 that can be oxidized at $850\text{ }^\circ\text{C}$ under oxygen, i.e., organic carbon (OC) and elemental
 250 carbon (EC), whereas AMS quantifies OA that consists of OC and the associated
 251 heteroatom (H, N, O, S ...). This fundamental difference engenders two major limitations
 252 for the assessment of fossil and non-fossil contributions of the OOA fractions. First, as
 253 the TC apportioned by ^{14}C measurements also included EC, assumptions related to the
 254 origins of the latter must be made. Furthermore, since the separation between EC and OC
 255 measured using the OC/EC instrument is method-dependent, biases associated with EC
 256 determination can impact the estimations. Second, the AMS measurement of OA includes
 257 heteroatom that can be unevenly distributed between the fossil carbon and the non-fossil
 258 carbon. Here also, this distribution was not empirically accessible and assumptions have
 259 to be made to calculate our estimations. Further uncertainties can arise from PMF
 260 calculations and residuals and from variability in the biomass $^{14}\text{C}/^{12}\text{C}$ ratio. The
 261 assumptions made to achieve the apportionment are explicitly presented in this section
 262 and the resulting biases and uncertainties are thoroughly discussed in section S.9.2.2.

263 The procedure went as follows: First, in order to estimate the fossil and non-fossil
 264 fractions of OC, EC was assumed to be entirely related to fossil carbon (assumption
 265 founded on Chemical Mass Balance calculations reported in El Haddad et al., 2011a).
 266 This is described in equations (2) and (3):

$$OC_f = TC_f - EC_f = TC_f - EC \left(EC_f = EC \parallel EC_{nf} = 0 \right) \quad (2)$$

$$OC_{nf} = TC_{nf} - EC_{nf} = TC_{nf} \left(EC_f = EC \parallel EC_{nf} = 0 \right) \quad (3)$$

267 Where TC_f , OC_f and EC_f correspond to the fossil TC, OC and EC, respectively, and
 268 TC_{nf} , OC_{nf} and EC_{nf} to the non-fossil TC, OC and EC, respectively.

269 The second step involved the transition from $PM_{2.5}OC$ measured on filter samples to
 270 PM_1OA determined by the AMS. This conversion was achieved for each of the samples
 271 by scaling OC_f and OC_{nf} to fossil OA (OA_f) and non-fossil OA (OA_{nf}), respectively, by
 272 a factor α :

$$OA_f = \alpha \times OC_f \quad (\alpha = PM_1OA / PM_{2.5}OC) \quad (4)$$

$$OA_{nf} = \alpha \times OC_{nf} \quad (\alpha = PM_1OA / PM_{2.5}OC) \quad (5)$$

273 where α is the ratio between AMS PM_1OA and filter $PM_{2.5}OC$. α is variable depending
 274 on the considered sample, but has an average of 0.92 ± 0.21 . The assumption underlying
 275 this scaling is that $PM_{2.5}OC$ and PM_1OA were associated with the same proportions of
 276 fossil and non-fossil mass (i.e. the ratio fossil/total was the same for $PM_{2.5}OC$ and
 277 PM_1OA). Biases arising from this assumption are discussed in the section S.9.2.2.

278 OA_f and OA_{nf} obtained in equations 4 and 5 can be accordingly expressed as a linear
 279 combination of the AMS/PMF OA fractions derived from fossil
 280 (fOA_i : POA_f , $SVOOA_f$ and $LVOOA_f$) and non-fossil ($nfOA_i$: POA_{nf} , $SVOOA_{nf}$ and
 281 $LVOOA_{nf}$) sources, respectively:

$$OA_f = \sum_i^l fOA_i = POA_f + SVOOA_f + LVOOA_f \quad (6)$$

$$OA_{nf} = \sum_i^m nfOA_i = POA_{nf} + SVOOA_{nf} + LVOOA_{nf} \quad (7)$$

282 where l and m are the total numbers of fOA_i and $nfOA_i$ fractions, respectively. As fOA_i
 283 and $nfOA_i$ are not directly accessible, equations 6 and 7 can be written in terms of the OA
 284 factors (OA_i) determined by AMS/PMF analysis and the respective share of fossil and
 285 non-fossil fractions to these factors such that

$$OA_f = \sum_i^l a_i \times OA_i = a_1 \times POA + a_2 \times SVOOA + a_3 \times LVOOA \quad \left(a_i = \frac{fOA_i}{fOA_i + nfOA_i} \right) \quad (8)$$

$$OA_{nf} = \sum_i^m b_i \times OA_i = b_1 \times POA + b_2 \times SVOOA + b_3 \times LVOOA \quad \left(b_i = \frac{nfOA_i}{fOA_i + nfOA_i} \right) \quad (9)$$

286 where a_i and b_i denote the relative share of fossil and non-fossil fractions to OA_i factors,
 287 respectively (a_1 for POA_f , a_2 for $SVOOA_f$, a_3 for $LVOOA_f$, b_1 for POA_{nf} , b_2 for
 288 $SVOOA_{nf}$ and b_3 for $LVOOA_{nf}$). This system of linear equations can be visualised as
 289 the following matrix equation:

$$\begin{bmatrix} POA & SVOOA & LVOOA & 0 & 0 & 0 \\ 0 & 0 & 0 & POA & SVOOA & LVOOA \\ 1 & 0 & 0 & 1 & 0 & 0 \\ 0 & 1 & 0 & 0 & 1 & 0 \\ 0 & 0 & 1 & 0 & 0 & 1 \end{bmatrix} \times \begin{bmatrix} a_1 \\ a_2 \\ a_3 \\ b_1 \\ b_2 \\ b_3 \end{bmatrix} = \begin{bmatrix} OA_f \\ OA_{nf} \\ 1 \\ 1 \\ 1 \end{bmatrix} \quad (10)$$

290 As POA was assumed to be strictly related to fossil sources
 291 (i.e. $POA_f = POA = HOA + F4$), the parameter a_1 can be assumed to equal 1, implying
 292 that b_1 equals 0 (i.e. $POA_{nf} = 0$), the sensitivity of the results to this assumption is
 293 assessed in section S.9.2.2). Equation 11 can be then simplified as follows:

$$\begin{bmatrix} SVOOA & LVOOA & 0 & 0 \\ 0 & 0 & SVOOA & LVOOA \\ 1 & 0 & 1 & 0 \\ 0 & 1 & 0 & 1 \end{bmatrix} \times \begin{bmatrix} a_2 \\ a_3 \\ b_2 \\ b_3 \end{bmatrix} = \begin{bmatrix} SOA_f \\ SOA_{nf} \\ 1 \\ 1 \end{bmatrix} \quad (11)$$

294 With SOA_f and SOA_{nf} denoting the fossil and non-fossil fractions of SOA, respectively,
 295 calculated as: $SOA_f = OA_f - POA_f$ and $SOA_{nf} = OA_{nf} - POA_{nf}$. The equations of the
 296 resulting linear system (equation 11) are not independent and thus the system has no
 297 solution. For that reason, a multiple linear regression analysis was applied instead to
 298 solve equation 11, which found the average values for a_i and b_i that fit best the equation,
 299 in the sense of solving the quadratic minimization problem. In equation 11
 300 AMS/PMF OA_i vectors were included as independent variables and OA_f and OA_{nf} as
 301 dependant variables.

302 It should be noted that the apportionment procedure followed here is not unique. As this
 303 study mainly focuses on AMS measurements, the chosen method is AMS data oriented in
 304 that the resulting apportionments would exhibit the same variability as the AMS/PMF

305 factors (e.g. $SVOOA_f + SVOOA_{nf} = SVOOA$). This is the result of the equation 11, in
 306 which AMS/PMF OA_i vectors were chosen as independent variables. As this equation is a
 307 self-consistent system (i.e. $OA_f + OA_{nf} - POA = SVOOA + LVOOA$), another approach is
 308 also possible; by considering OA_f and OA_{nf} as independent variables, this second
 309 approach yields the same average results but orients the variability towards ^{14}C
 310 measurements.

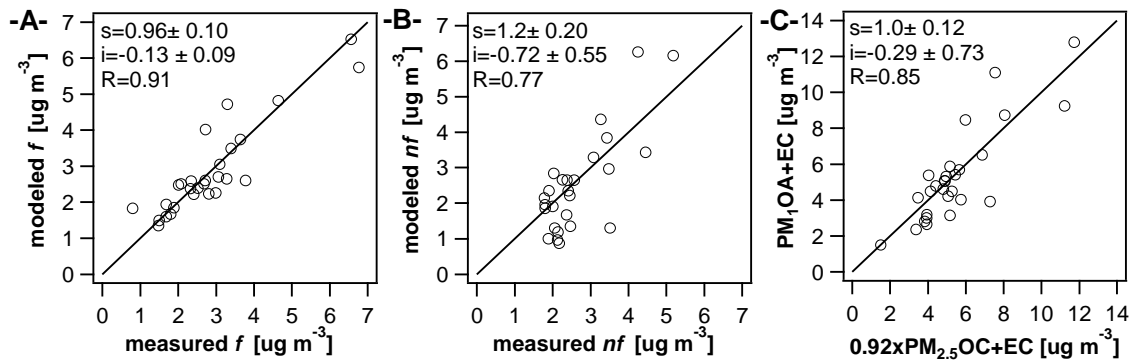
311 S.9.2 Output quality control, uncertainty assessments and potential biases

312 S.9.2.1 Output quality control and residual analyses

313 One of the major drawbacks of the multiple regression analysis applied here is that it
 314 considers a constant contribution of fossil and non-fossil sources to each of the
 315 OA_i factors (i.e., constant a_i and b_i ratios), while these contributions may significantly
 316 vary over the course of the measurements. Accordingly, a_i and b_i ratios should be
 317 regarded as average contributions of fossil and non-fossil sources to OA_i . These ratios are
 318 reported in Tab.S1.

Tab.S1: a_i and b_i ratios for the POA, SVOOA and LVOOA fractions.

	POA	SVOOA	LVOOA
a_i	1.0	0.33 ± 0.11	0.082 ± 0.085
b_i	0.0	0.67 ± 0.11	0.92 ± 0.08

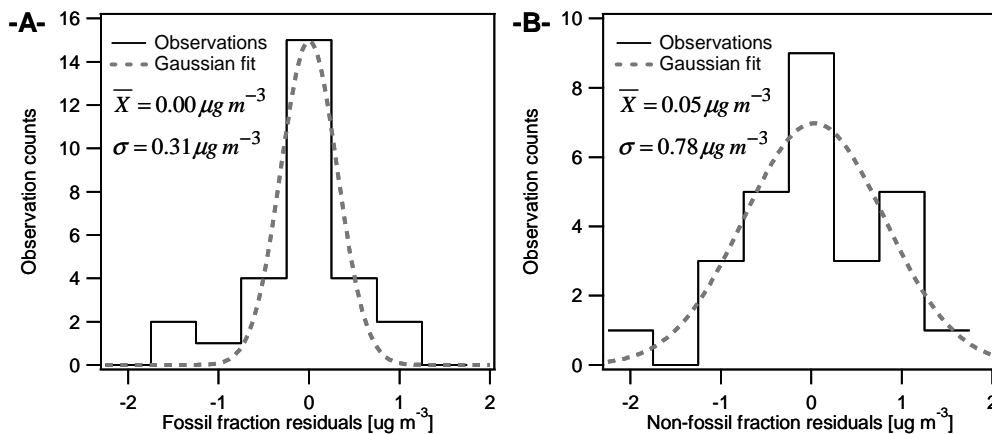


319 **Fig.S8:** Scatter plots of modelled vs. measured data for the fossil (A) and non-fossil (B) fractions.
 320 Measured fossil fraction= $EC+0.92 \times OC_f$, modelled fossil fraction= $EC+HOA+F4+$
 321 $SVOOA_f+LVOOA_f$, Measured non-fossil fraction= $0.92 \times OC_f$, and modelled fossil fraction=
 322 $SVOOA_{nf}+LVOOA_{nf}$. The 0.92 value is the average value of the factor α used in equations 6 and
 323 7. The comparison between filter measurements and AMS measurements is shown in panel C.
 324

325 For all panels, the slope of the linear regression (s), its intercept (i) and its coefficient of
326 determination (R) are also indicated (n=28 samples for each plot).

327 Fig.S8 compares the measured and the modelled concentrations for the total fossil and
328 non-fossil fractions. It shows that the model captured quite well the amounts and the
329 variability of the measured concentrations, especially in the case of the fossil fraction
330 (Fig.S8a). In the case of the non-fossil fraction, the model tended to slightly
331 underestimate (overestimate) the measured levels at low (high) concentrations (Fig.S8b).
332 It should be noted though that most of the variability observed in panels A and B of
333 Fig.S8 arose from discrepancies between the AMS PM_{10} OA and filter-based $PM_{2.5}$ OC, as
334 shown in panel C of the same figure. Differences between the 2 measurement techniques
335 were accounted for in equations 4 and 5 prior to the multiple regression analyses by the
336 coefficient α that encompasses various conversion factors. Overall, these comparisons
337 validated the representativeness of a_i and b_i obtained in the multiple regression analyses.

338



339

340 **Fig.S9:** Residuals' normal distributions (modelled – measured) derived from the multiple
341 regression approach applied above for the fossil (A) and the non-fossil (B) fractions. Residuals
342 are fitted using a Gaussian fit, from which the mean (\bar{X}) and the standard deviation (σ) are
343 calculated for both fractions.

344 Assumptions underlying the residuals' distributions were examined for the fossil and
345 non-fossil fractions in Fig.S9. Residuals followed normal distributions with mean values
346 statistically equal to zero, implying that errors are homoscedastic (variance = 0) and are
347 not correlated. From Fig.S9, it is possible to estimate the uncertainties related to the total
348 fossil and non-fossil OA fractions. Fossil and non-fossil OA were accordingly estimated

349 to contribute $1.52 \pm 0.31 \mu\text{g m}^{-3}$ (implying 20% of errors) and $2.52 \pm 0.78 \mu\text{g m}^{-3}$ (implying
350 31% of errors), respectively. These uncertainties included: (1) measurement differences
351 between filter-based $\text{PM}_{2.5}$ TC and AMS PM_1 OA + EC (Fig.S8c) and (2) variability in
352 a_i and b_i obtained in the multiple regression analyses (see the related uncertainties in
353 Tab.S1).

354 **S.9.2.2 General assessment of uncertainties and biases**

355 It is worthwhile to note that a great part of the uncertainties assessed for the absolute
356 concentrations of fossil and non-fossil OA arose from discrepancies between AMS and
357 filter measurements and hence is not representative of the statistical significance of each
358 of the fractions. The statistical significance of the relative contributions of HOA, F4,
359 SVOOA_f , LVOOA_f , SVOOA_{nf} and LVOOA_{nf} were assessed through a sensitivity test
360 using a random selection technique. Inputs to the calculation are the PMF factor mass
361 concentrations, ^{14}C data, and OC/EC measurements. The calculation was performed
362 based on equations (2-11) and proceeded as follows:

- 363 ○ For each of the input parameters a range was assigned, within which these can
364 vary (see Tab.S2). The criteria on which we based our assessment of these ranges
365 are developed below, in Appendix A.
- 366 ○ The parameters were then allowed to randomly vary within the range
367 predetermined in the previous step, assuming a normal distribution. This approach
368 is somewhat similar to Monte Carlo calculations and allows vast numbers of
369 combinations of input parameters to be computed (McKay et al., 1979). A Monte
370 Carlo simulation would involve testing all possible combinations of input
371 parameters, which would be prohibitive in terms of processing time. In contrast,
372 random sampling is much more effective and for our purposes provided
373 essentially the same results as a full Monte Carlo analysis (McKay et al., 1979).
- 374 ○ Following the approach described above, 50 sets of parameters were generated
375 randomly and used subsequently in the equations 2-11 to calculate the inputs for
376 the multiple linear regression analysis (i.e. SOA_f , SOA_{nf} , SVOOA and LVOOA).
377 This provided for each set of parameters average values for a_i and b_i plus the
378 corresponding uncertainties.

379 ○ For each set of the coefficients a_i and b_i previously generated, the average values
380 of these coefficients were varied assuming a binomial distribution, derived based
381 on the corresponding uncertainties provided by the multiple linear regression
382 analyses. In this step and for each set of parameters, ten values were generated for
383 a_i and b_i and used to compute the contributions of $SVOOA_f$, $LVOOA_f$, $SVOOA_{nf}$
384 and $LVOOA_{nf}$. This gave in total 500 different solutions.

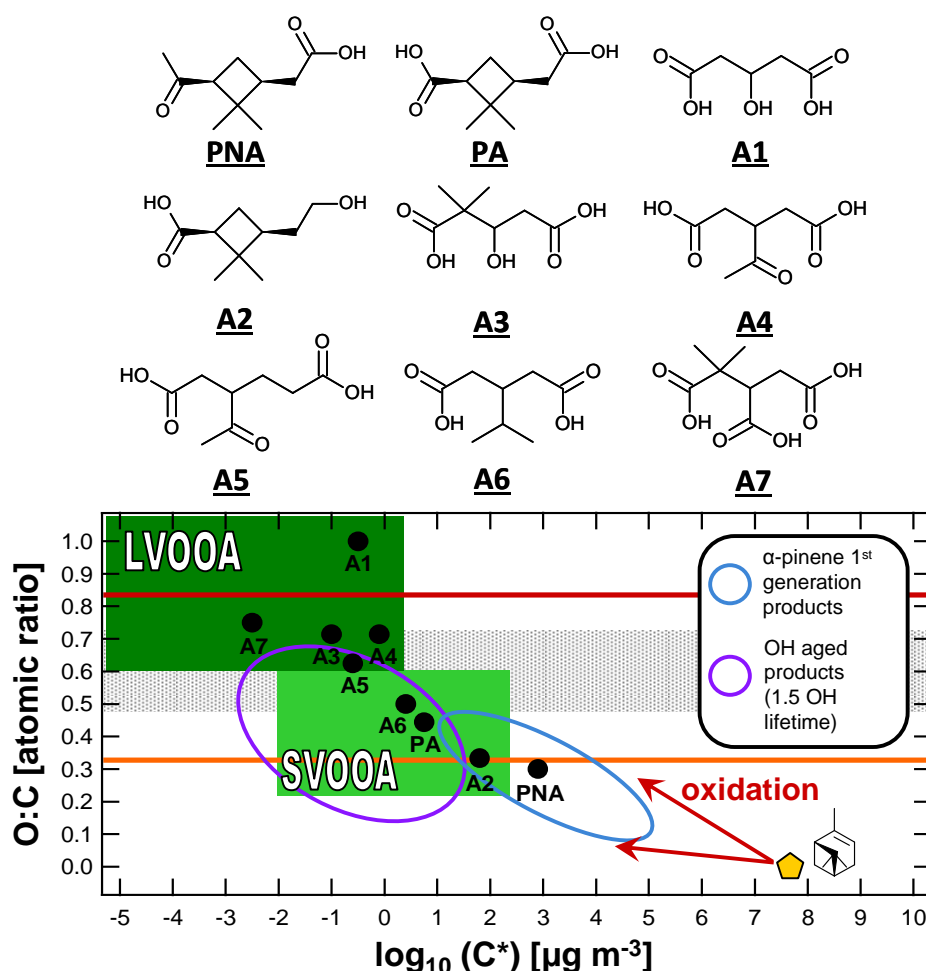
385 A great advantage of this approach is that combinations of parameters which are very
386 unlikely (e.g., that only the minimum-possible values from each parameter were used)
387 will represent only a small percentage of the output. The obtained 500 solutions are
388 presented graphically as a probability density (frequency distribution) of possible
389 solutions to the source apportionment problem we have set up, as shown in Fig.7 in the
390 manuscript.

391 This analysis provided strong support for our results, allowing the assessment of the
392 uncertainties underlying our measurements and assumptions and offering a measure of
393 our ability to separate the different components (statistical significance of each
394 component). It showed that the uncertainties of our estimations depend on the component
395 considered. Depending strictly on the PMF analysis errors, the uncertainties associated
396 with the contributions of POA (HOA and F4) were less than 10%. Conversely, for OOA
397 components the uncertainties were less homogenous. For non-fossil OOAs the
398 uncertainties were around 10% as these were well resolved by the regression model,
399 whereas for fossil OOAs uncertainties are higher (~36% and ~58% for $SVOOA_f$ and
400 $LVOOA_f$, respectively), as these were poorly resolved by the regression model and
401 strongly dependant on the EC measurements and the assumptions made for POA. All 6
402 fractions were statistically significant with contributions higher than 0 (Z equal 23, 7.4,
403 2.8, 1.7, 9.2, 12 for HOA, F4, $SVOOA_f$, $LVOOA_f$, $SVOOA_{nf}$ and $LVOOA_{nf}$ respectively,
404 with $Z = \text{average/uncertainty}$).

405 Additionally, the sensitivity test offered the assessment of the biases on the
406 apportionments presented in the manuscript. The sensitivity test results suggest that we
407 might underestimate the contributions of F4, HOA, $SVOOA_{nf}$ and $LVOOA_f$ by 9%, 6%,
408 5% and 23%, respectively and overestimate the $SVOOA_f$ and $LVOOA_{nf}$ by 34% and 5%,
409 respectively. The main conclusion to be derived from this analysis is the robustness of the

410 results presented and discussed in the manuscript. For example, OOA_{nf} was clearly the
 411 biggest contributor to OA. It is also clear that LVOOA was derived predominately from
 412 non-fossil precursors ($\text{LVOOA}_{\text{nf}}/\text{LVOOA}=89\pm 7\%$), whereas SVOOA included a larger
 413 fraction of fossil SOA ($\text{SVOOA}_{\text{nf}}/\text{SVOOA}=75\pm 8\%$). Given the wide range of
 414 uncertainties used in the sensitivity test, these results demonstrate that, in general, we can
 415 clearly identify the contribution from different components.

416 **S.10 Distribution of the α -pinene oxidation products in the 2D-VBS**



417

418 **Fig.S10:** 2D-framework for α -pinene SOA aging adapted from Jimenez et al., 2009, representing
 419 OA oxidation state (approximated by O:C) vs. OA volatility ($\log_{10}(\text{C}^*)$ at 298 K). The ambient
 420 OOA factors are represented in this 2D space by the 2 green squares, with LV-OOA being less
 421 volatile and more oxidized than SV-OOA (Jimenez et al., 2009). First generation products from
 422 α -pinene (yellow pentagon) + ozone reaction are distributed according to the blue contour.
 423 Products derived from subsequent OH oxidation (1.5 OH lifetimes) of first generation products
 424 are represented with purple contour (Jimenez et al., 2009). This oxidation reproduces a substantial
 425 shift toward ambient LV-OOA volatility and oxidation state. We added on this 2D space α -pinene
 426 first and subsequent generation oxidation products measured in this study by GC/MS (PNA, PA

427 and A1-A7). The volatilities of these compounds were calculated using the approach proposed by
428 Donahue et al., 2011. O:C ratios of pure SV-OOA and LV-OOA retrieved by AMS/PMF2
429 analysis were calculated following the parameterization proposed in Aiken et al. (2009) and
430 indicated by the orange and dark red lines, respectively. Following the same methodology, the
431 range of O:C ratios ($0.48 < \text{O:C}_{\text{OOA}} < 0.72$) of total OOA encountered during the measurement
432 period was determined and indicated by the dotted area.
433

434 **Appendix A:** Calculations of the different parameters entered as inputs in the sensitivity test

435 For the parameters in Tab.S2, the ranges were established as follows:

436 ■ For EC/OC measurements, the range was designed to encompass biases and uncertainties

437 associated with the separation between EC and OC. This range was bounded by

438 measurements determined following NIOSH and EUSAAR2 protocols, respectively. For

439 EC and OC, a constant bias between the 2 protocols was determined to be $40\pm 8\%$ and

440 $6\pm 5\%$.

441 ■ The average uncertainty for the discrimination between fossil and non-fossil TC was 4%,

442 including uncertainties in ^{14}C measurements and errors due to the correction for ^{14}C

443 inputs from the bomb testing.

444 ■ An assumption made in equations 4 and 5 relates to the origin of EC, which was

445 estimated to only pertain to the fossil fraction. This assumption would bias high the

446 contributions of fossil sources to the secondary OC fractions. As there was little influence

447 from biomass burning, we assumed an upper limit contribution of non-fossil sources to

448 EC to be 15%, (based on Minguillón et al., 2011 and references), and varied this

449 contribution between 0 and 15%.

Tab.S2: Ranges [Low, High] of the different parameters entered as inputs to the uncertainty calculation. E* denotes equations 2-11.

E*	Parameters	Variables	Low	High	Remarks
2, 3	OC_f, OC_{nf}	OC/EC	NIOSH	EUSAAR2	
		F_f	$0.96 \times F_{nf}$	$1.04 \times F_{nf}$	Uncertainties on measurements of ^{14}C in TC
		EC_f	$0.85 \times EC$	EC	Origin of EC: $EC = EC_f + EC_{nf}$
4, 5	$\alpha = PM_1OA/PM_{2.5}OC$ see Tab.S3	α_1^{OC}	0.76	0.88	Diameter cut-offs: $\alpha_1^{OC} = PM_1OC/PM_{2.5}OC$
		α_2^{OC}	CI(-)	CI(+)	Positive artefacts based on Fig.S3: CI(-) and CI(+) are the upper and lower bounds of the confident interval on the linear regression
8,9	AMS/PMF2 OA	<i>Factors</i>	<i>FPEAK0</i>	<i>FPEAK1</i>	AMS/PMF2 results obtained for FPEAKs between 0 and 1.
10,11	POA_f, POA_{nf}	$a_1 \times POA$	$0.75 \times HOA + F4$	$0.9 \times HOA + F4$	$a_1 \times POA$ is the fraction of fossil POA. Its uncertainty is constrained based on Fig.S7

450 ■ The conversion from $PM_{2.5}OC$ measured on filter samples to PM_1OA determined by the

451 AMS was performed in equations 2 and 3, using a common factor α (with $\alpha =$

452 $PM_1OA/PM_{2.5}OC$) for both fossil and non-fossil OC. This factor encompassed three key

453 corrections related to differences between the two measurement techniques, including

454 differences in diameter cut-offs between AMS and filter sampling (referred to

455 as $PM_1OC/PM_{2.5}OC$ ratio), the adsorption artefacts on the filters, and the OM/OC ratio.
 456 The assumption underlying the $PM_{2.5}OC$ to PM_1OA conversion is that the aggregate of
 457 the aforementioned corrections was similar for both fossil and non-fossil OC and well
 458 represented by α . Indeed, these corrections can vary greatly between the primary and the
 459 secondary fractions, which exhibited variable contributions to the fossil and non-fossil
 460 OC. To address the biases resulting from the application of a single conversion factor α ,
 461 the latter is deconvolved in equation (12) into several factors, such that

$$PM_1OA = \alpha \times PM_{2.5}OC = \sum_i^n \left(\prod_j^p \alpha_{ij} \right) \times OC_i \quad (12)$$

462 In this equation, α_{ij} denotes the factor used for a conversion (j) applied to an OC_i
 463 fraction. n is the total number of OC fractions; in our case, it was limited to two fractions
 464 representing the primary and the secondary OC. p is the total number of α_i conversions
 465 applied to OC_i ; in our case, p was equal to 3, accounting for the $PM_1OC/PM_{2.5}OC$
 466 ratio ($j=1$), for the sampling artefacts ($j=2$) and for the OM/OC ratio ($j=3$). The following
 467 is an example performed for the campaign average value, representing the matrix of
 468 α_{ij} factors for primary and secondary OC (Tab.S3). Similar calculations were performed
 469 for all of the data set to complete the sensitivity test. In this calculation, α_{ij} were
 470 measured for the total OC (α_j^{OC}), assumed for the primary OC (α_j^{POC}), and inferred
 471 for secondary OC (α_j^{SOC}). The different conversions include the following:

472 - α_1^{OC} denotes the $PM_1OC/PM_{2.5}OC$ ratio, estimated using size resolved OC
 473 measurements, i.e., $0.82 \pm 0.06\%$. POC was assumed to pertain entirely to the PM_1
 474 fraction ($\alpha_1^{POC} = 1$), resulting in an α_1^{SOC} of 0.77 (i.e. 77% of the $PM_{2.5}$ SOC are included
 475 in the PM_1 fraction).

476 - α_2^{OC} is the ratio allowing the correction for the sampling artefacts retrieved from
 477 Fig.S3, with an average value of 0.72. Artefacts were assumed to be evenly distributed
 478 between the primary and the secondary fractions, i.e. $\alpha_2^{POC} = \alpha_2^{SOC}$ (Tab.S3).

479 - α_3^{OC} is the OM/OC ratio, obtained from the comparison between PM_1 AMS and LPI
 480 measurements. An average α_3^{OC} value of 1.67 was found, and assuming an α_3^{POC} value
 481 of 1.2 for primary OC a value of 1.81 can be inferred for the α_3^{SOC} .
 482

Tab.S3: α_{ij} factors estimated for POC, SOC and total OC fractions.

α_{ij}	α_j^{POC}	α_j^{SOC}	α_j^{OC}
α_{i1}	1.0	0.77	0.82
α_{i2}	0.72	0.72	0.72
α_{i3}	1.20	1.81	1.67
$\prod_j^p \alpha_{ij}$	0.84	0.98	0.95

483 From α_{ij} matrix, overall conversion factors $\prod_j^p \alpha_{ij}$ can be inferred for POC, SOC and total
 484 OC, which were equal to 0.84, 0.98 and 0.95, respectively. Estimated $\prod_j^p \alpha_j^{OC}$ (0.95) is
 485 comparable to the average α empirically determined and used in equations (4) and (5) to
 486 convert from $PM_{2.5}OC$ measured on filter samples to PM_1OA determined by the
 487 AMS ($\alpha = 0.92 \pm 0.21$).

488 Using $\prod_j^p \alpha_j^{POC}$ and $\prod_j^p \alpha_j^{SOC}$ obtained above, one can apply different conversion factors
 489 to POA and SOA. In the sensitivity test such a calculation has been made by considering
 490 a range of α_1^{OC} and α_2^{OC} (Tab.S3).

- 491 ■ In the calculation of equations 10 and 11, we considered for the apportionments the
 492 AMS/PMF2 results, including *POA*, *SVOOA* and *LVOOA*. One approach to assess the
 493 uncertainties on the AMS/PMF2 apportionments consists of varying FPEAK within a
 494 reasonable range, in our case between FPEAK =0 and FPEAK =1.
- 495 ■ In the calculation of equations 10 and 11, we considered that POA pertains only to the
 496 fossil fraction. However, we observed evidence of inputs from cooking (a non fossil
 497 primary source) to the HOA factor. To take this observation into account in the

498 uncertainty calculations, we considered that these cooking inputs contributed between
499 10% and 25% of total HOA, based on Fig.S7.

500

501

502

503 **References**

- 504 Agrawal, H., Welch, W. A., Miller, J. W., and Cocker, D. R.: Emission measurements from a crude oil
505 tanker at sea, *Environ. Sci. Technol.*, 42, 7098–7103, 2008.
- 506 Aiken, A. C., DeCarlo, P. F., Kroll, J. H., Worsnop, D. R., Huffman, J. A., Docherty, K. S., Ulbrich, I. M.,
507 Mohr, C., Kimmel, J. R., Sueper, D., Sun, Y., Zhang, Q., Trimborn, A., Northway, M., Ziemann, P.
508 J., Canagaratna, M. R., Onasch, T. B., Alfarra, M. R., Prevot, A. S. H., Dommen, J., Duplissy, J.,
509 Metzger, A., Baltensperger, U., and Jimenez, J. L.: O/C and OM/OC Ratios of Primary, Secondary,
510 and Ambient Organic Aerosols with HighResolution Time-of-Flight Aerosol Mass Spectrometry,
511 *Environ. Sci. Technol.*, 42, 4478–4485, doi:10.1021/es703009q, 2008.
- 512 Baduel, C., Voisin, D., and Jaffrezo, J. L.: Comparison of analytical methods for HULIS measurements in
513 atmospheric particles, *Atmos. Chem. Phys.*, 9, 5949–5962, doi:10.5194/acp-9-5949-2009, 2009.
- 514 Baduel, C., Voisin, D., and Jaffrezo, J. L.: Seasonal variations of concentrations and optical properties of
515 water soluble HULIS collected in urban environments, *Atmos. Chem. Phys.*, 10, 4085–4095,
516 doi:10.5194/acp-10-4085-2010, 2010.
- 517 Bae, M.-S., Schauer J.J., DeMinter, J.T., Turner, J.R., Smith, D. and Cary, R.A.: Validation of a semi-
518 continuous instrument for elemental carbon and organic carbon using a thermal-optical method, *Atmos.*
519 *Environ.*, 38, 2885–2893, 2004.
- 520 Cavalli, F., Viana, M., Yttri, K. E., Genberg, J., and Putaud, J.-P.: Toward a standardised thermal-optical
521 protocol for measuring atmospheric organic and elemental carbon: the EUSAAR protocol, *Atmos.*
522 *Meas. Tech.*, 3, 79–89, doi:10.5194/amt-3-79-2010, 2010.
- 523 Chauvel, C., Bureau, S., and Poggi, C.: Comprehensive chemical and isotopic analyses of basalt and
524 sediment reference materials, *Geostand. Geoanalyt. Res.*, 35, 125–143, doi:10.1111/j.1751-
525 908X.2010.00086., 2010.
- 526 Chirico, R., A.S.H. Prevot, P.F. DeCarlo, M.F. Heringa, R. Richter, E. Weingartner, and Urs Baltensperger.
527 Aerosol and Trace Gas Vehicle Emission Factors Measured in a Tunnel Using an Aerosol Mass
528 Spectrometer and other On-line Instrumentation. *Atmospheric Environment*, 45(13), 2182-2192,
529 2011.
- 530 Donahue, N. M., Kroll, J. H., Pandis, S. N., Robinson, A. L.: A two-dimensional volatility basis set – Part
531 2: Diagnostics of organic-aerosol evolution, *Atmos. Chem. Phys. Discuss.*, 11, 24883–24931,
532 doi:10.5194/acpd-11-24883-201, 2011.
- 533 Drewnick, F., Hings, S. S., DeCarlo, P., Jayne, J.T., Gonin, M., Fuhrer, K., Weimer, S., Jimenez, J.L.,
534 Demerjian, K.L., Borrmann, S., Worsnop, D.R.: A new time-of-flight aerosol mass spectrometer
535 (TOF-AMS) – Instrument description and first field deployment, *Aerosol Sci. Tech.*, 39, 637–658,
536 2005.

537 El Haddad, I., Marchand, N., Dron, J., Temime-Roussel, B., Quivet, E., Wortham, H., Jaffrezo, J. L.,
538 Baduel, C., Voisin, D., Besombes, J. L., and Gille, G.: Comprehensive primary particulate organic
539 characterization of vehicular exhaust emissions in France, *Atmos. Environ.*, 43, 6190–6198, 2009.

540 El Haddad, I., Marchand, N., Wortham, H., Piot, C., Besombes, J. -L., Cozic, J., Chauvel, C., Armengaud,
541 A., Robin, D., Jaffrezo, J. -L., Primary sources of PM_{2.5} particles in an industrial Mediterranean
542 city, Marseille, *Atmospheric Chemistry and Physics*, 11, 2039–2058, 2011a.

543 El Haddad, I., Marchand, N., Temime-Roussel, B., Wortham, H., Piot, C., Besombes, J. -L., Baduel, C.,
544 Voisin, D., Armengaud, A., Jaffrezo, J. -L., Insights into the secondary fraction of the organic
545 aerosol in a Mediterranean urban area: Marseille, *Atmospheric Chemistry and Physics*, 11, 2059–
546 2079, 2011b.

547 Fine, P. M., Cass, G. R., and Simoneit, B. R. T.: Chemical Characterization of Fine Particle Emissions from
548 the Fireplace Combustion of Woods Grown in the Southern United States, *Environ. Sci. Technol.*,
549 36, 1442–1451, doi:10.1021/es0108988, 2002.

550 Jimenez, J. L., Canagaratna, M. R., Donahue, N. M., Prevot, A. S. H., Zhang, Q., Kroll, J. H., DeCarlo, P.
551 F., Allan, J. D., Coe, H., Ng, N. L., Aiken, A. C., Docherty, K. S., Ulbrich, I. M., Grieshop, A. P.,
552 Robinson, A. L., Duplissy, J., Smith, J. D., Wilson, K. R., Lanz, V. A., Hueglin, C., Sun, Y. L., Tian,
553 J., Laaksonen, A., Raatikainen, T., Rautiainen, J., Vaattovaara, P., Ehn, M., Kulmala, M.,
554 Tomlinson, J. M., Collins, D. R., Cubison, M. J., Dunlea, E. J., Huffman, J. A., Onasch, T. B.,
555 Alfarra, M. R., Williams, P. I., Bower, K., Kondo, Y., Schneider, J., Drewnick, F., Borrmann, S.,
556 Weimer, S., Demerjian, K., Salcedo, D., Cottrell, L., Griffin, R., Takami, A., Miyoshi, T.,
557 Hatakeyama, S., Shimono, A., Sun, J. Y., Zhang, Y. M., Dzepina, K., Kimmel, J. R., Sueper, D.,
558 Jayne, J. T., Herndon, S. C., Trimborn, A. M., Williams, L. R., Wood, E. C., Middlebrook, A. M.,
559 Kolb, C. E., Baltensperger, U., and Worsnop, D. R.: Evolution of organic aerosols in the atmosphere,
560 *Science*, 326, 1525–1529, 2009.

561 Levin, I., Kromer, B., Schochfischer, H., Bruns, M., Munnich, M., Berdau, D., Vogel, J. C., and Munnich,
562 K. O.: 25 Years of Tropospheric C-14 Observations in Central-Europe, *Radiocarbon*, 27, 1-19, 1985.

563 Levin, I., and Heshaimer, V.: Radiocarbon - A unique tracer of global carbon cycle dynamics,
564 *Radiocarbon*, 42, 69-80, 2000.

565 Minguillón, M. C., Perron, N., Querol, X., Szidat, S., Fahrni, S. M., Alastuey, A., Jimenez, J. L., Mohr, C.,
566 Ortega, A. M., Day, D. A., Lanz, V. A., Wacker, L., Reche, C., Cusack, M., Amato, F., Kiss, G., Hoffer,
567 A., Decesari, S., Moretti, F., Hillamo, R., Teinilä, K., Seco, R., Peñuelas, J., Metzger, A., Schallhart, S.,
568 Müller, M., Hansel, A., Burkhardt, J. F., Baltensperger, U., and Prévôt, A. S. H.: Fossil versus
569 contemporary sources of fine elemental and organic carbonaceous particulate matter during the DAURE

570 campaign in Northeast Spain, *Atmos. Chem. Phys.*, 11, 12067-12084, doi:10.5194/acp-11-12067-2011,
571 2011.

572 McKay, M. D., Beckman, R. J. and Conover, W.J.: A Comparison of Three Methods for Selecting Values
573 of Input Variables in the Analysis of Output from a Computer Code, *Technometrics*, 21, 239-245, 1979.

574 Middlebrook, A.M., Bahreini, R., Jimenez, J.L. and Canagaratna M.R.: Evaluation of Composition-
575 Dependent Collection Efficiencies for the Aerodyne Aerosol Mass Spectrometer using Field Data.
576 *Aerosol Science and Technology*, DOI:10.1080/02786826.2011.620041, 46, 258–271, 2012

577 Rolph, G. D.: Real-time Environmental Applications and Displays System (READY) Website
578 (<http://ready.arl.noaa.gov>). NOAA Air Resources Laboratory, Silver Spring, MD, 2010.

579 Rogge, W. F., Hildemann, L. M., Mazurek, M. A., Cass, G. R., and Simoneit, B. R. T.: Sources of Fine
580 Organic Aerosol .4. Particulate Abrasion Products from Leaf Surfaces of Urban Plants, *Environ. Sci.*
581 *Technol.*, 27, 2700–2711, 1993a.

582 Rogge, W. F., Hildemann, L. M., Mazurek, M. A., Cass, G. R., and Simoneit, B. R. T.: Sources of Fine
583 Organic Aerosol.5. Natural Gas Home Appliances, *Environ. Sci. Technol.*, 27, 2736–2744, 1993b.

584 Schmid, H., Laskus, L., Jurgen Abraham, H., Baltensperger, U., Lavanchy, V., Bizjak, M., Burba, P.,
585 Cachier, H., Crow, D., Chow, J., Gnauk, T., Even, A., ten Brink, H. M., Giesen, K.-P., Hittenberger, R.,
586 Hueglin, C., Maenhaut, W., Pio, C., Carvalho, A., Putaud, J.-P., Toom-Sauntry, D., and Puxbaum, H.:
587 Results of the “carbon conference” international aerosol carbon round robin test stage I, *Atmos.*
588 *Environ.*, 35, 2111–2121, 2001.

589 Tsai, J.-H., Lin, K.-H., Chen, C.-Y., Ding, J.-Y., Choa, C.-G., and Chiang, H.-L.: Chemical constituents in
590 particulate emissions from an integrated iron and steel facility, *J. Hazard. Mater.*, 147, 111–119, 2007.

591 Watson, J. G., Robinson, N. F., Fujita, E. M., Chow, J. C., Pace, T. G., Lewis, C., and Coulter, T.: CMB8
592 Applications and Validation Protocol for PM_{2.5} and VOCs, US EPA, USA, 1998.

593 Weitkamp, E. A., Lipsky, E. M., Pancras, P. J., Ondov, J. M., Polidori, A., Turpin, B. J., and Robinson, A.
594 L.: Fine particle emission profile for a large coke production facility based on highly time-resolved
595 fence line measurements, *Atmos. Environ.*, 39, 6719–6733, 2005.

596